THE ASTROPHYSICAL JOURNAL, 465:815–824, 1996 July 10

A $C^{18}O$ SURVEY OF DENSE CLOUD CORES IN TAURUS: CORE PROPERTIES

TOSHIKAZU ONISHI, AKIRA MIZUNO, AKIKO KAWAMURA, HIDEO OGAWA, AND YASUO FUKUI
Department of Astrophysics, Nagoya University, Chikusa-ku, Nagoya 464-01, Japan; ohnishi, mizuno, kawamura, ogawa, fukui@a.phys.nagoya-u.ac.jp
Received 1995 September 13; accepted 1996 January 24

ABSTRACT

This paper discusses observational results of physical properties of dense cores in the Taurus complex. The observations were carried out in the $C^{18}O$ ($J = 1$–0) line at a linear resolution of 0.1 pc with the 4 m millimeter radio telescope at Nagoya University. Based on the previous ^{13}CO observations of Mizuno et al. (1995) as a guide map, we obtained 7200 spectra (8 deg^2) at a 2′ grid spacing, corresponding to more than 90% of the area whose molecular column density is greater than 3.5×10^{21} cm^{-2}. The total molecular mass of the $C^{18}O$ cloud is estimated to be 2900 $M_\odot$, which is 43% of the mass of the ^{13}CO cloud. About 97% of the $C^{18}O$ spectra have an optical depth smaller than 0.5, and the $C^{18}O$ emission is optically thin over almost all the region at a size scale down to $\sim$0.1 pc. The basic structure of the $C^{18}O$ cloud is clumpy. We identified 40 dense cores of $n(H_2) \sim 10^4$ cm^{-3}, whose mass ranges from 1 to 80 $M_\odot$. The average physical parameters of the $C^{18}O$ cores are as follows: radius 0.23 pc, line width 0.49 km s^{-1}, column density 6.9×10^{21} cm^{-2}, and mass 23 $M_\odot$. The mass spectrum of the cores, dN/dM versus M, is fitted by a power law with an index of -0.9 ± 0.2, which is significantly smaller than those of the previous surveys. Most of the cores are spatially elongated; the average aspect ratio is 1.8, and the direction of the major axis of the cores tends to be perpendicular to the typical direction of the optical polarization vectors. An analysis of correlations among the physical quantities of the cores indicates that the line width has a positive correlation with the mass and the column density but not with the size. Most of the cores are roughly gravitationally bound and at least approximately in virial equilibrium.

Subject headings: ISM: clouds — ISM: individual (Taurus Cloud Complex) — ISM: molecules — ISM: structure — radio lines: ISM

1. INTRODUCTION

A dense molecular cloud core is considered to be a site of star formation. Molecular gas will contract gravitationally at some regions within a molecular cloud to form dense cores leading to star formation and dissipation of the core after stellar birth. The average molecular number density of dense cores is $\geq 10^4$ cm^{-3}, which is greater than that of the background molecular cloud by more than an order of magnitude. In order to understand the whole process of star formation, it is important to have a comprehensive understanding of the evolution of dense cores. An investigation of low-mass star-forming regions is appropriate for such a study, because low-mass young stars evolve much more slowly than high-mass young stars and because the number of low-mass stars is much larger than that of high-mass stars. Therefore, it is very important to have a complete set of molecular data on dense cores in a low-mass star-forming region.

A survey for dense cores using molecular lines was made by Myers, Linke, & Benson (1983). They selected visually opaque regions from the Palomar Sky Prints and observed 70 regions in the ^{13}CO and $C^{18}O$ molecular lines. Later, they extended their observations in the NH_3 line (Benson & Myers 1989). They presented maps of 41 cores and showed that 68% of the cores had *IRAS* point sources (*IRAS* Point Source Catalog version 2, 1988) which are considered to be protostellar objects or T Tauri stars (Beichman et al. 1986). These observations and others in other spectral lines confirmed that a dense core is an actual star formation site.

The Taurus-Auriga cloud complex contains a few tens of cataloged dark clouds (Barnard 1927; Lynds 1962) located near the solar system at a distance of 140 pc (Elias 1978). There are $\sim$100 PMS (pre–main-sequence) stars in this region (Elias 1978; Cohen & Kuhi 1979; Jones & Herbig 1979; Herbig & Bell 1988), and the complex is one of the most typical low-mass star-forming regions. The mass of the PMS stars is around 0.7 $M_\odot$ (Cohen & Kuhi 1979; Herbig & Bell 1988). The Taurus region is not affected by external shocks or ultraviolet radiation because there are no massive stars or supernova remnants around it. Therefore, this region is most suitable for studying the earliest stages of the spontaneous formation of low-mass stars.

Tens of dark clouds within the Taurus complex were observed in various molecular lines; e.g., ^{12}CO (Ungerechts & Thaddeus 1987), ^{13}CO (Schloerb & Snell 1984; Duvert, Cernicharo, & Baudry 1986; Nercessian et al. 1988), $C^{18}O$ (Cernicharo & Guelin 1987), and CS (Zhou et al. 1989). Ungerechts & Thaddeus covered the whole Taurus region at half a degree angular resolution in the ^{12}CO ($J = 1$–0) line and revealed an overall distribution of the molecular clouds. The ^{12}CO line, however, was not suitable for tracing a star-forming region because the optical depth was too large, and the spatial resolution of 1.2 pc was too coarse. On the other hand, the ^{13}CO ($J = 1$–0) line is a good tracer of dense clouds because it is optically thin over most of the cloud. Mizuno et al. (1995, hereafter Paper I) carried out a survey for dense molecular clouds in the Taurus complex in the ^{13}CO ($J = 1$–0) line (see also Fukui et al. 1991, 1994). They observed $\sim$40 deg^2 with a grid spacing of 2′. This survey revealed the structure of the dense molecular gas of the whole region at a spatial resolution of 0.1 pc, and thus provided a rich knowledge of the molecular clouds that likely lead to star formation.

Even the ^{13}CO spectra, however, tend to be saturated toward high-density regions, making it difficult to understand the detailed distribution of high-density cores. In this

paper, we present results of a survey for dense cores in the $C^{18}O$ ($J = 1$–0) line at 2.7 mm wavelength in Taurus to study star formation in a dense cloud core. The abundance of the $C^{18}O$ molecule is less than that of ^{13}CO molecule by a factor of ~ 5 if the terrestrial abundance is assumed, and the $C^{18}O$ spectra are thus not saturated even toward high-density regions at a scale of ≥ 0.1 pc. Although the spectral lines like CS ($J = 2$–1) and $H^{13}CO^+$ ($J = 1$–0) (Mizuno et al. 1994) trace even denser regions, their spectral intensities are weaker by a factor of ~ 3 than the $C^{18}O$ intensities, so they are too weak to be used for mapping in a reasonably short observing time. Therefore, $C^{18}O$ is the best spectral line to obtain a complete data set of dense cores in nearby star-forming regions. Although there are some observations in the $C^{18}O$ line in the other regions like Ophiuchus (Nozawa et al. 1991; Willking & Lada 1983) and Orion (Dutrey et al. 1991), there was no extensive survey in $C^{18}O$ for the whole extent of a low-mass star-forming region. We discuss here the overall physical properties of the $C^{18}O$ clouds and the cores. Comparison between the $C^{18}O$ cores properties and young stellar objects (YSOs) is a subject of a forthcoming paper (Onishi et al. 1996).

2. OBSERVATIONS

The $C^{18}O$ ($J = 1$–0) observations were carried out with the 4 m radio telescope at Nagoya University during the winter seasons of 1992 through 1995. The front end was a superconducting Nb mixer receiver (Ogawa et al. 1990), with a typical system temperature of 150 K (single-sideband), including the atmosphere toward the zenith. The acousto-optic spectrometer, which has 1664 channels with a 40 MHz bandwidth and a 40 kHz resolution, provided a velocity resolution of 0.1 km s^{-1} at 110 GHz. To achieve the rms noise fluctuations of 0.2 K (T_r^*) per channel, an integration time of 1–2 minutes was needed under typical good weather conditions in Nagoya. The observations were made by the frequency-switching method whose switching interval was 13 MHz (35 km s^{-1} at 110 GHz). The telescope had a full beam width at a half-maximum of 2.7 (0.11 pc at 140 pc) at 109.782182 GHz, the frequency of the $C^{18}O$ ($J = 1$–0) transition. The mapping was made with a grid spacing of 2′ (0.08 pc at 140 pc). The spectral intensity was corrected for the atmospheric absorption by using the chopper wheel method. We observed TMC-1A [$\alpha(1950) = 4^h38^m42^s$, $\delta(1950) = 25°45'35''$] every 2 hours and used it as a calibration standard. We assumed that the $C^{18}O$ radiation temperature T_r^* toward TMC-1A is 2 K (e.g., Myers et al. 1983).

It is difficult to survey the whole Taurus molecular cloud in a few years even with the existing best receivers because the typical intensity of the $C^{18}O$ ($J = 1$–0) line is weaker than that of the ^{13}CO line by a factor of 3–5. To obtain a sample of dense cores in $C^{18}O$ effectively within a limited time, we used the ^{13}CO map (Paper I) as a guide map. We observed around 7200 points (8 deg^2), corresponding to more than 90% of the area whose molecular column density derived from the ^{13}CO observations is greater than 3.5×10^{21} cm^{-2} (^{13}CO integrated intensity of 6 K km s^{-1}). The total area which we covered is outlined in the ^{13}CO map (Fig. 1).

In addition, we observed ^{12}CO ($J = 1$–0) emission toward 41 localized $C^{18}O$ peaks in order to estimate the excitation temperature of the $C^{18}O$ transition in 1994 January. We assume that the ^{12}CO emission is optically thick and that the excitation temperature of $C^{18}O$ is the same as that of ^{12}CO. The mean, maximum, and minimum excitation temperatures derived from the peak temperatures of the ^{12}CO spectra are 10.2, 12.9, and 8.3 K, respectively, and the standard deviation is estimated to be 1.2 K. Thus, we adopt the excitation temperature of the CO ($J = 1$–0) transition as 10 K to calculate column densities in the present work.

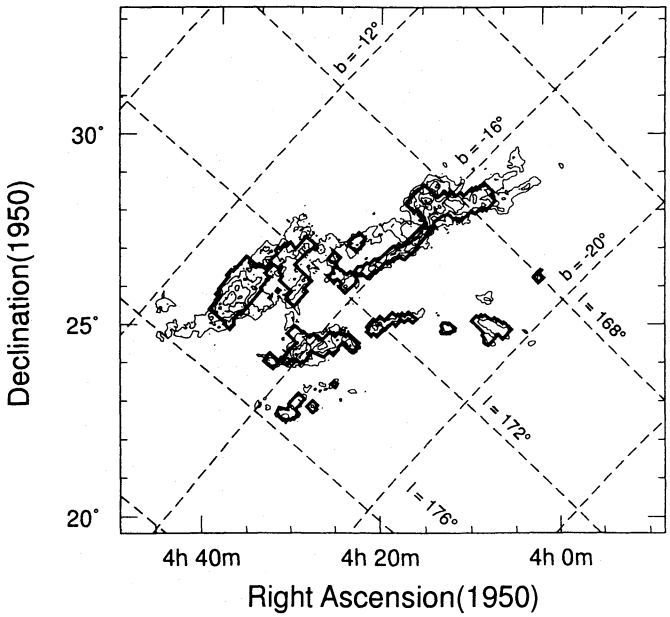

FIG. 1.—Thick solid lines show the observed area superposed on the contour map of ^{13}CO integrated intensity (Paper I). Lowest contour level and contour interval are 3.0 K km s^{-1} and 2.0 K km s^{-1}, respectively.

3. RESULTS

Figure 2 (Plate 7) shows a map of the $C^{18}O$ integrated intensity which covers 8 deg^2 in the Taurus region. The overall structure of the $C^{18}O$ clouds is more clumpy and filamentary than that of the ^{13}CO clouds. There are three massive clouds in the following regions: (1) $l = 173°$–$175°$ and $b = -14°$ to $-13°$ (known as HCL2), (2) $l = 167°$–$171°$ and $b = -17°$ to $-15°$ (L1495, B213, and B217), and (3) $l = 173°$–$174°$ and $b = -17°$ to $-16°$ (B18). The latter two regions have filamentary structures, although the former one has a ringlike shape. There are about 15 isolated clouds around these three massive clouds.

In order to calculate the optical depth of a $C^{18}O$ spectrum as a function of frequency, v(Hz), we used the following equation:

$$\tau_v(C^{18}O) = -\ln\left[\left[\frac{1 - T_R^*(v)(\mathrm{K})}{5.3(\mathrm{K})} \times \left\{\frac{1}{\exp\left[5.3(\mathrm{K})/T_{ex}(\mathrm{K})\right] - 1} - 0.17\right\}^{-1}\right]\right] \quad (1)$$

To derive the $C^{18}O$ column density of each observed point, we assume that the rotational levels of $C^{18}O$ ($J = 1$–0) are thermalized. Several spectra have an unsymmetrical shape or a multipeaked profile. Although different velocity components in a multipeaked profile may come from different regions in the line of sight, we assumed tentatively that these components come from a single cloud. We divide a spectrum into 0.1 km s^{-1} bins to calculate the H_2 column

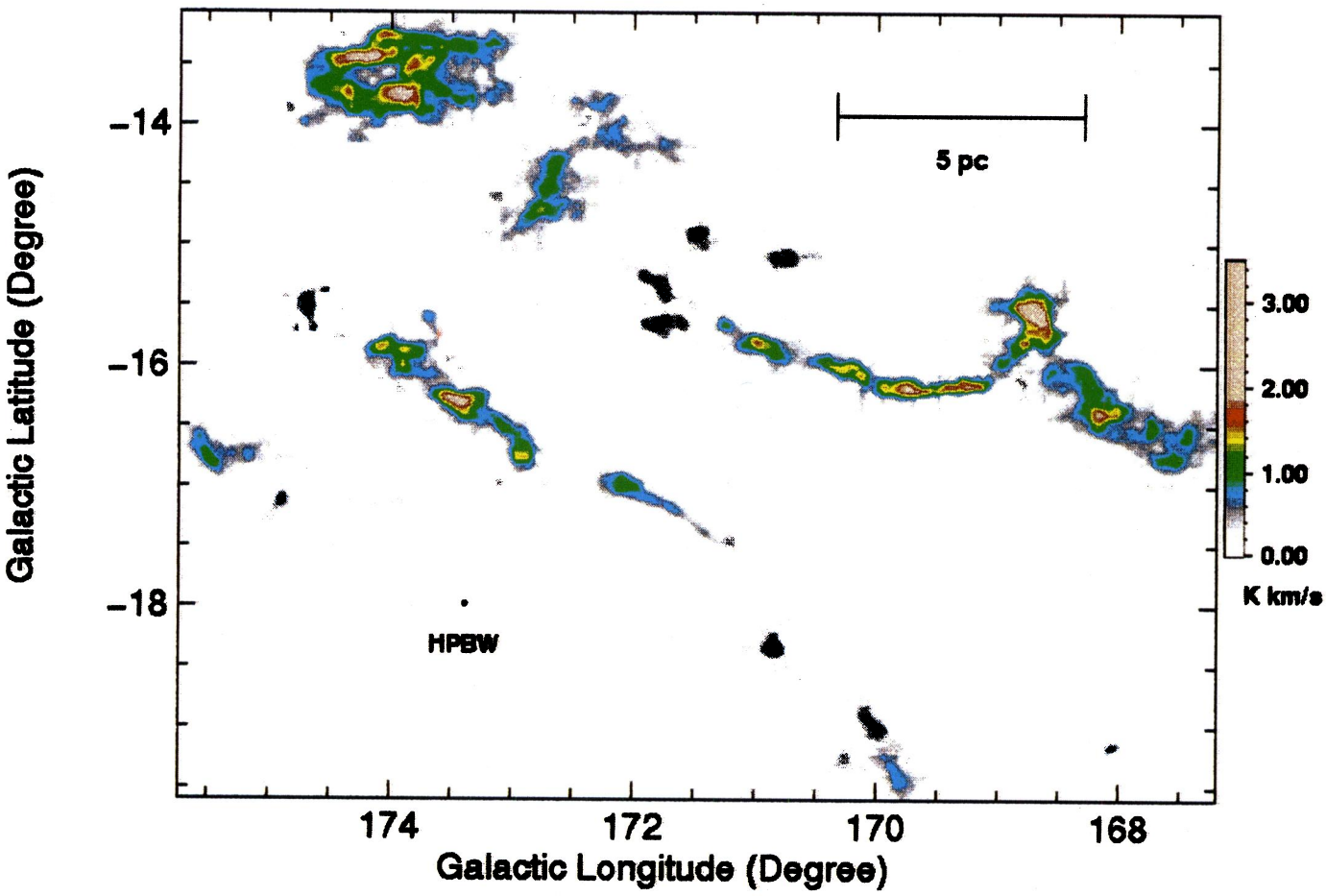

FIG. 2.—False color $C^{18}O$ total intensity (K km s^{-1}) map of the Taurus molecular cloud in Galactic coordinates

ONISHI et al. (see 465, 816)

density within each bin and sum them up within a velocity range in which the $C^{18}O$ intensity is larger than 3 σ in order to derive $C^{18}O$ column density, $N(C^{18}O)$, using the following equation:

$$N(C^{18}O) = 2.4 \times 10^{14} \sum_i \frac{\tau_{v_i}(C^{18}O) \times 0.1(\text{km s}^{-1})}{\{1 - \exp[-5.3(\text{K})/T_{ex}(\text{K})]\}} (\text{cm}^{-2}) . \quad (2)$$

We calculated $N(H_2)$ from $N(C^{18}O)$ by using the equation of Frerking, Langer, & Wilson et al. (1982) for $N(C^{18}O) > 3 \times 10^{14}$ cm^{-2}. Their estimated errors of the equation in the slope and offsets are $\pm$ 30% and $\pm$ 100%, respectively, and therefore the error of mass due to the conversion would be less than a factor of 2. The mean molecular weight is assumed to be equal to 2.3. The total mass of the clouds is estimated to be 2900 $M_\odot$, which corresponds to 43% of the ^{13}CO cloud mass of 6800 $M_\odot$ (Paper I). The emissions that have a $C^{18}O$ integrated intensity of <3 σ were ignored when we calculated the total mass of $C^{18}O$ clouds.

3.1. $C^{18}O$ *Core*

To characterize a density enhancement of a molecular cloud, we defined a $C^{18}O$ "core." The procedures to identify the cores are the following: (1) find a peak position in $C^{18}O$ integrated intensity, (2) draw a contour at a level of half the peak intensity and identify it as a core unless it contains previously identified cores, (3) find a local intensity peak in the integrated intensity outside the previously identified cores, and (4) go back to procedure (2) until the peak integrated intensity is lower than 5 σ (0.7 K km s^{-1}). We exclude the cores that have only one observed point. By using this method, we identified 40 cores within the observed region, as shown in Figure 3. It is noted that Figure 3 is a total velocity-integrated map. If a spectrum has a multi-peaked profile that is completely separated in velocity, we assume that the different velocity components correspond to the clouds that have different distance in the line of sight. Although there is a peak near $l = 172.9$, $b = -16.7$ in Figure 3, the emissions have a double-peaked profile which is completely separated in velocity. One component has the same velocity as core 19, but there is no core around $l = 172.9$, $b = -16.7$ that satisfies the criteria of the core with this velocity. The peak integrated intensity of the other component is lower than 5 σ. Therefore, we do not identify the peak around $l = 172.9$, $b = -16.7$ in the total integrated intensity map as a core. Table 1 shows the physical properties of the cores. We tentatively classified the cores into nine regions; L1495, L1489, B213, L1498, L1521, L1506, B18, HCL2, and L1536, as given in column (14).

3.1.1. *Line Width and Spectral Shape*

About 85% of the spectra appear to be well approximated to a single Gaussian shape, judged by eyes, although the rest are very unsymmetric or multipeaked. Most multipeaked profiles cannot be separated into different components accurately because the separation in velocity is small ($\lesssim$2 km s^{-1}). Therefore, we fit tentatively all the spectra with a single Gaussian function to derive the line widths of a spectrum of cores.

The line width (FWHM) of a core was defined as that derived from a Gaussian fitting at the peak intensity posi-

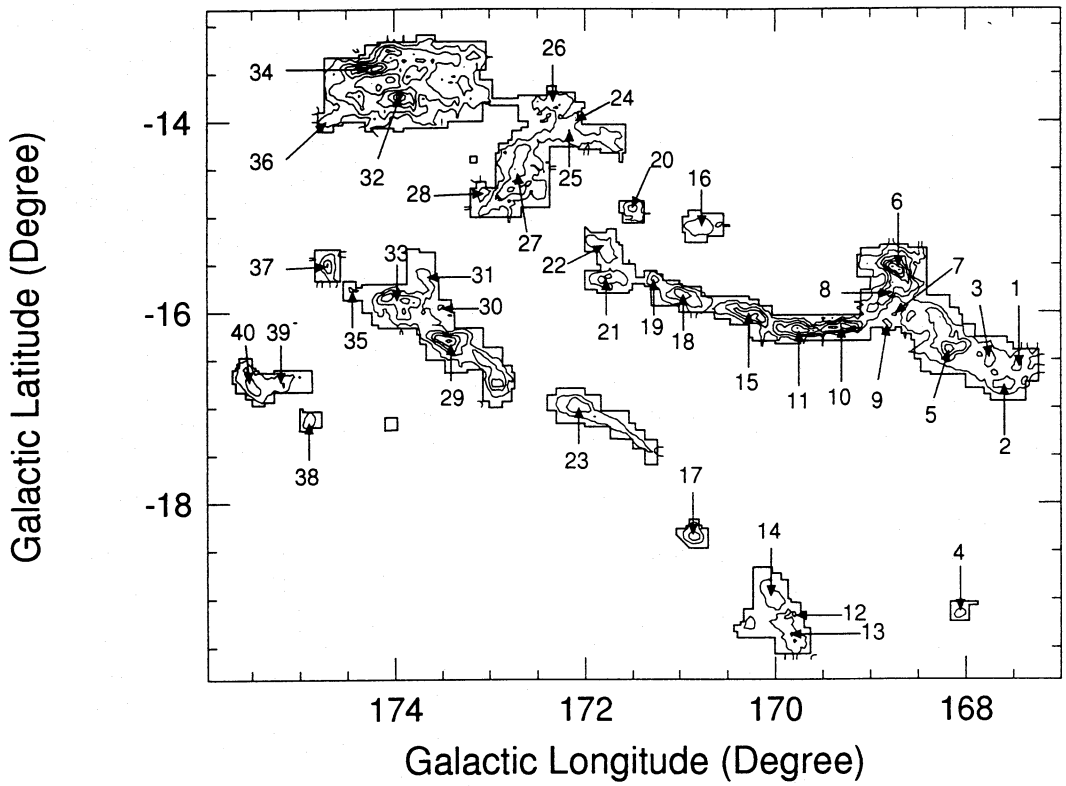

FIG. 3.—The positions of the cores selected are indicated on the $C^{18}O$ integrated intensity map. Solid lines show the observed area. Lowest contour level and contour interval are 0.42 K km s^{-1} and 0.42 K km s^{-1}, respectively.

TABLE 1

CATALOG OF $C^{18}O$ CORES IN TAURUS

Core No.	Position[a] L (°)	B (°)	RA(1950) (h,m)	DEC(1950) (°, ′)	Mass ($M_\odot$)	Radius[b] (pc)	Tr* (K)	Δv (km/s)	$N(H_2)$ ($10^{21}cm^{-2}$)	$n(H_2)$[c] (10^3cm^{-3})	Aspect ratio[d]	P. A. (degree)	Region
1	167.47	-16.57	04 08.1	28 25	14.9	0.20	1.98	0.43	6.3	7.6	1.3		L1495
2	167.57	-16.77	04 07.8	28 13	27.2	0.28	1.76	0.41	6.1	5.3	1.9	90	L1495
3	167.77	-16.47	04 09.3	28 18	16.6	0.21	2.24	0.37	6.7	7.8	1.3		L1495
4	168.07	-19.17	04 01.7	26 11	4.6	0.13	1.64	0.50	4.7	8.6	1.0		L1489
5	168.17	-16.40	04 10.8	28 04	47.3	0.29	2.80	0.71	9.8	8.2	1.7	-80	L1495
6	168.73	-15.53	04 15.3	28 17	55.6	0.25	3.96	0.75	15.5	15.0	2.0	50	L1495
7	168.73	-16.03	04 13.7	27 56	1.5	0.08	0.74	0.86[e]	4.0	12.1	1.3		L1495
8	168.83	-15.77	04 14.8	28 03	9.6	0.13	1.58	0.99[e]	9.6	17.8	1.3		L1495
9	168.83	-16.10	04 13.8	27 49	3.7	0.12	0.94	1.02[e]	4.3	8.4	2.0	50	L1495
10	169.23	-16.17	04 14.7	27 30	35.6	0.24	2.46	1.94[ef]	10.6	10.7	2.2	90	B213
11	169.60	-16.20	04 15.7	27 13	46.0	0.28	2.12	1.46[e]	10.0	8.6	3.2	90	B213
12	169.80	-19.17	04 06.8	25 01	1.1	0.07	0.92	0.43[e]	4.4	16.5	1.0		L1498
13	169.87	-19.37	04 06.4	24 50	24.5	0.28	2.22	0.33	5.3	4.6	2.0	30	L1498
14	170.07	-18.97	04 08.2	24 58	21.9	0.28	2.08	0.32	4.8	4.1	1.8	40	L1498
15	170.30	-16.03	04 18.4	26 51	43.6	0.30	1.84	0.74	8.2	6.5	3.1	70	B213
16	170.73	-15.13	04 22.6	27 09	19.5	0.27	2.20	0.40	4.8	4.3	1.4		L1521
17	170.87	-18.37	04 12.5	24 51	10.8	0.17	2.76	0.41	6.7	9.7	1.0		L1498
18	171.00	-15.80	04 21.2	26 30	34.9	0.27	2.80	0.63	8.0	7.1	2.1	60	B213
19	171.27	-15.67	04 22.4	26 24	10.1	0.17	2.18	0.59	5.8	8.1	1.3		B213
20	171.50	-14.90	04 25.6	26 45	9.4	0.16	2.62	0.46	6.3	9.6	1.1		L1521
21	171.73	-15.60	04 23.9	26 07	15.6	0.21	2.36	0.35	6.3	7.4	1.6	-80	B213
22	171.93	-15.27	04 25.6	26 12	21.4	0.28	2.06	0.39	4.8	4.2	2.5	50	B213
23	172.10	-17.03	04 20.3	24 54	37.1	0.32	2.58	0.49	6.4	4.9	2.4	60	L1506
24	172.10	-13.97	04 30.5	26 56	1.8	0.07	1.34	0.51[f]	7.2	26.5	1.3		L1521
25	172.20	-14.07	04 30.4	26 48	20.2	0.25	1.68	0.85[f]	5.6	5.5	1.1		L1521
26	172.43	-13.83	04 31.9	26 47	17.6	0.24	1.58	0.90[e]	5.5	5.6	1.7	-70	L1521
27	172.87	-14.77	04 30.0	25 51	80.5	0.45	2.24	0.37	6.8	3.7	2.9	-20	L1521
28	173.06	-14.77	04 30.5	25 43	8.4	0.19	0.98	0.61[e]	4.0	5.1	1.7	-30	L1521
29	173.40	-16.30	04 26.3	24 27	45.7	0.27	3.08	0.62	11.2	10.2	1.5	70	B18
30	173.53	-15.97	04 27.8	24 35	2.2	0.09	1.06	0.77[e]	4.4	11.6	1.0		B18
31	173.70	-15.57	04 29.6	24 43	12.2	0.21	1.66	0.60[e]	4.7	5.4	2.0	40	B18
32	173.93	-13.73	04 36.4	25 45	49.9	0.26	3.62	0.94[f]	12.6	11.6	2.3	80	HCL2
33	174.03	-15.83	04 29.7	24 19	49.7	0.32	2.76	0.58	8.3	6.3	1.2		B18
34	174.37	-13.43	04 38.7	25 36	68.3	0.32	3.06	0.84[f]	11.7	8.9	4.6	90	HCL2
35	174.47	-15.73	04 31.2	24 03	4.7	0.14	1.46	0.62[e]	4.2	7.3	1.6	80	B18
36	174.70	-14.00	04 37.6	25 00	9.2	0.17	1.82	0.38	5.3	7.4	1.8	-60	HCL2
37	174.70	-15.50	04 32.6	24 02	11.5	0.17	2.56	0.55	7.1	10.3	1.4		B18
38	174.87	-17.10	04 27.7	22 52	6.9	0.15	1.44	1.16[e]	5.1	8.0	1.3		L1536
39	175.20	-16.73	04 29.9	22 52	8.4	0.17	1.46	0.79[f]	5.2	7.5	1.0		L1536
40	175.47	-16.83	04 30.3	22 36	26.9	0.27	2.26	0.45	6.4	5.7	2.4	30	L1536

[a] The position that has the largest integrated intensity in the core.
[b] The radius of circle having the same area as the area of the core.
[c] Assuming the shape of the core as a sphere.
[d] Major axis divided by minor axis of the core.
[e] $\sigma(\Delta v) \geq 0.05$ km s^{-1}.
[f] Apparently multipeaked profile.

tion. We exclude the data whose line width errors calculated from the covariance are larger than 0.05 km s^{-1} when we use the line width to discuss the physical properties of the cores. Apparently multipeaked or unsymmetrical profiles (cores 10, 24, 25, 32, 34, and 39) were also not considered in the discussion regarding line width. Under the criteria above, the $C^{18}O$ line width (Fig. 4*a*) is distributed between 0.32 km s^{-1} (core 14 in L1498) and 0.75 km s^{-1} (core 6 in L1495), with a mean line width of 0.49 km s^{-1}. Thus, the observed line width is at least a factor of 3 larger than the thermal width assuming kinetic temperature of 10 K. In Figure 5 we show the three spectra at the peak of $C^{18}O$ cores: a single-peaked profile (core 33), a multipeaked profile (core 34), and the profile which has the lowest $C^{18}O$ intensity (core 28).

3.1.2. *Column Density*

We calculated the column densities for all the observed points within a core using equations (1) and (2), and then we averaged them up within the core. We define the molecular column density of a core as the average column density within a half-intensity contour of the core. The H_2 column densities derived from the $C^{18}O$ observations are distributed from 4.0×10^{21} cm^{-2} (core 7 in L1495) to 1.6×10^{22} cm^{-2} (core 6 in L1495) (Fig. 4*b*). The mean H_2 column density is estimated to be 6.9×10^{21} cm^{-2}.

3.1.3. *Size and Shape*

The size of a core is defined as a radius of the circle that has the same area as the core. The radius ranges from 0.07 pc (core 12 in L1498) to 0.45 pc (core 27 in L1521) (Fig. 4*c*). The mean radius is estimated to be 0.23 pc. The aspect ratio of the core is defined as the major axis divided by the minor axis. The lengths of the major and minor axes were measured by hand. This ratio range from 1.0 (circular) to 4.6 (core 34 in HCL2) (Fig. 4*d*), and its mean value is estimated to be 1.8. Thus, the cores have an elongated shape. We also measured a position angle of the major axis of the core whose aspect ratio is larger than 1.25. The position angle of the core whose major axis is perpendicular to the galactic

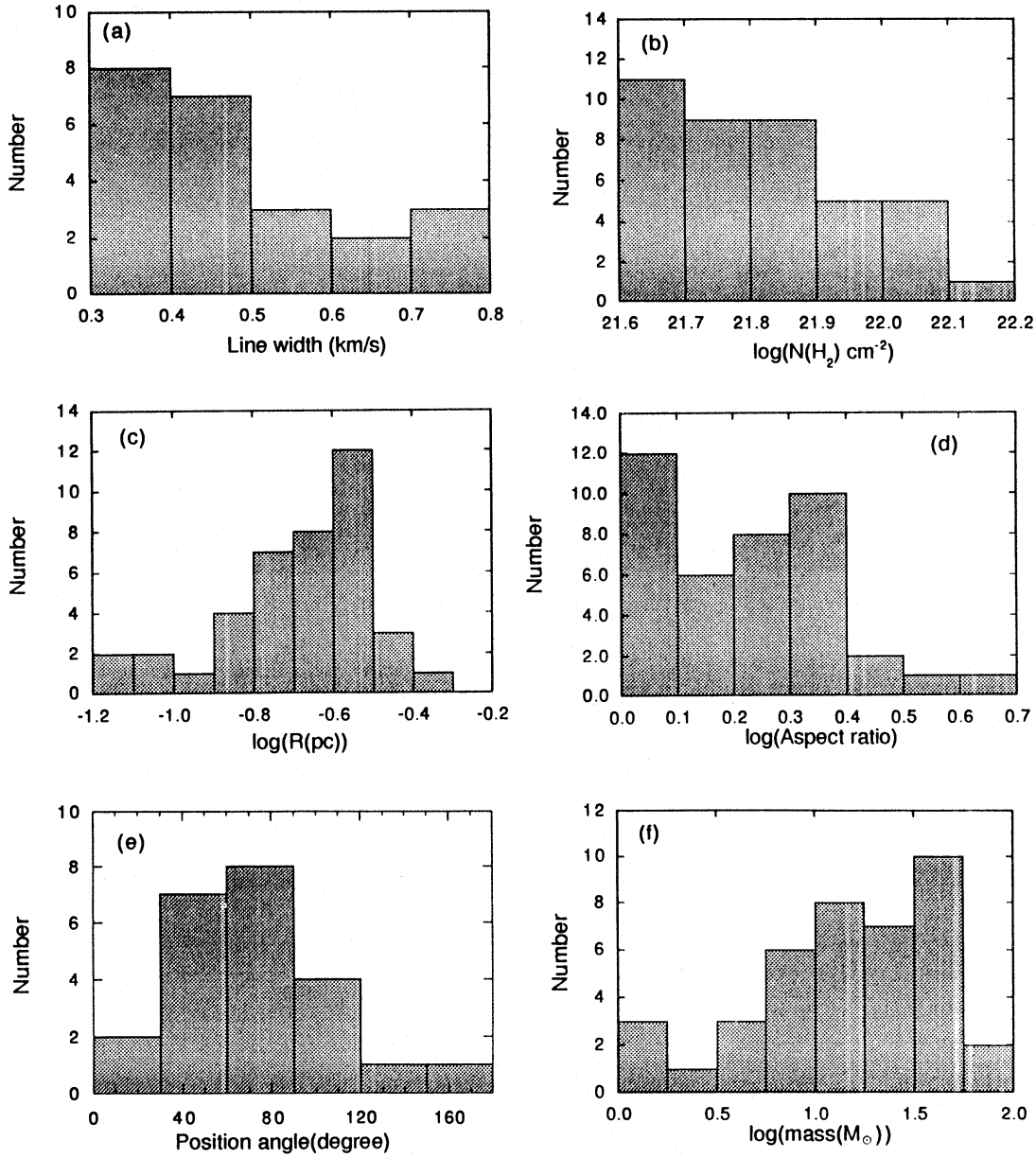

FIG. 4.—Histograms of the core properties. (*a*) Line width with σ (line width) < 0.05 km s^{-1}, (*b*) column density, (*c*) radius, (*d*) axial ratio, (*e*) position angle, and (*f*) mass of the cores.

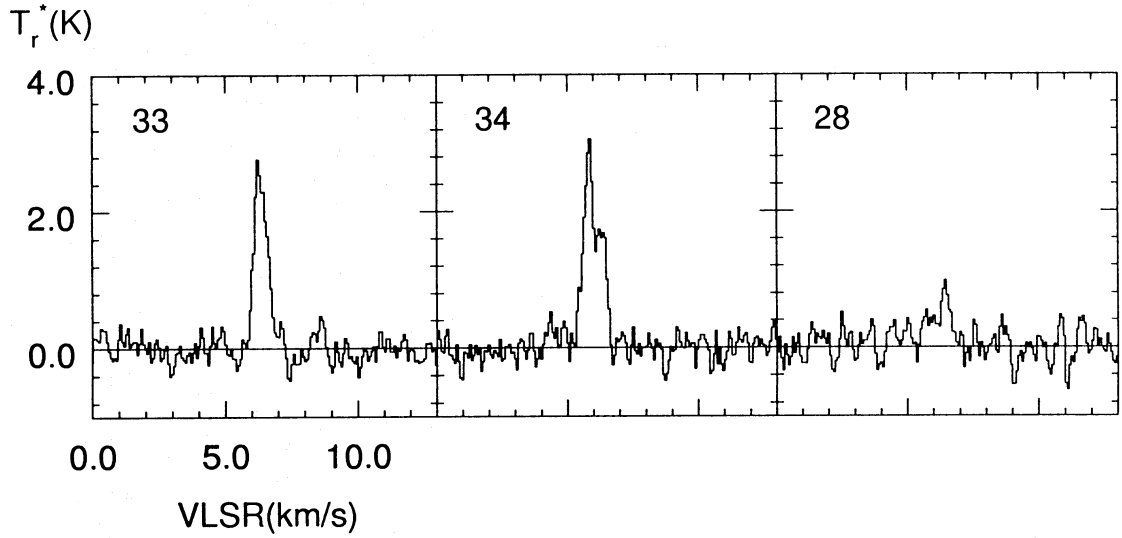

FIG. 5.—Sample spectra at the peak of C^{18}O cores: a single-peaked profile (core 33), a multipeaked profile (core 34), and the profile with the lowest C^{18}O intensity (core 28).

plane is defined as 0°, increasing counterclockwise up to 90°. Figure 4*e* shows the distribution of the position angle, and the distribution has a peak at around 70°.

3.1.4. *Mass and Mass Spectrum*

The mass of a core was derived by summing up the column densities for all the observed points within a half-intensity contour of the core and ranges from 1.1 $M_\odot$ (core 12 in L1498) to 80.5 $M_\odot$ (core 27 in L1521) (Fig. 4*f*). The mean value is estimated to be 23 $M_\odot$. The detection limit was derived by assuming a core which has the smallest mass in our criteria and is estimated to be ~ 1 $M_\odot$. The average number density of a core was calculated from the radius and the mass by assuming that the core has a spherical shape and ranges from 3.7×10^3 cm^{-3} (core 27 in L1521) to 2.7×10^4 cm^{-3} (core 24 in L1521). The mean H_2 density is estimated to be 8.6×10^3 cm^{-3}. The error of the number density is considered to be larger than those of the other quantities, since most of the cores do not have a spherical shape, as discussed above. For the smallest cores like numbers 7, 12, 24, and 27 which may not be resolved with the present observations, the number density is uncertain because the estimation of the size contains a larger error.

Figure 6 shows the core mass spectrum, dN/dM versus M. The number density of cores decreases with mass for all the mass range. We adopt a mass of 3 $M_\odot$ as a conservative limit in calculating the mass spectrum in order to ensure completeness in sampling. For the cores which have the mass of > 3 $M_\odot$, the mass spectrum is fitted by a power law of $\log(dN/dM) \propto \gamma \log M$ with $\gamma = -0.9 \pm 0.2$ by assuming $N^{1/2}$ counting uncertainties.

3.2. *Individual Regions*

We present briefly the cloud and core properties of individual regions.

L1495.—The total mass of the eight cores (numbers 1, 2, 3, 5, 6, 7, 8, and 9) in this region is estimated to be 176 $M_\odot$, which is 28% of the total mass of gas in the region estimated from $C^{18}O$ observations (hereafter we shall refer to the total mass for each region), 637 $M_\odot$. This is the region whose column density is largest in the whole observed region. Several parts in the cloud have double peaked $C^{18}O$ profiles, which is explained by the fact that the cloud has several filamentary components of different velocities (Paper I). The denser parts have a larger line width of ~ 0.7 km s^{-1}. The line width decreases considerably to 0.4 km s^{-1} in the outer part of the cloud.

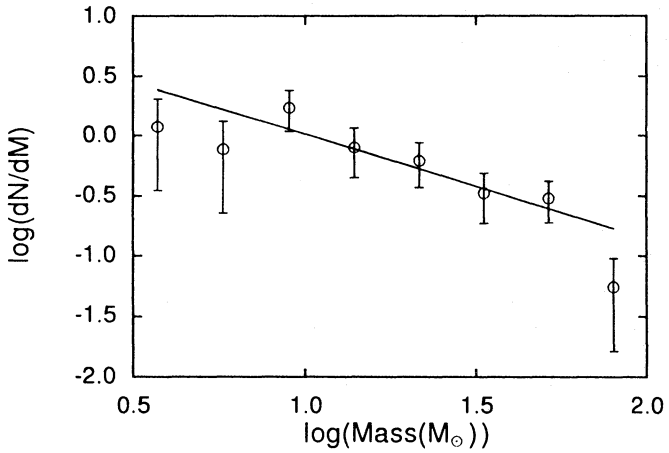

FIG. 6.—Mass spectrum for the cores. Here dN/dM is the number of cores per solar mass interval. The error bar indicates only $N^{1/2}$ counting uncertainties. The straight line represents the best fit for $M > 3M_\odot$ by a power law $dN/dM \propto M^{-0.9}$.

L1489.—There is only one core in this region, and the mass of the core (number 4) is estimated to be 4.6 $M_\odot$, which is 88% of the total mass, 5.2 $M_\odot$. The core is also round-shaped in several lines: NH_3 (Benson & Myers 1989), CS (Zhou et al. 1989), and ^{13}CO (Paper I).

B213.—The total mass of the seven cores in this region (numbers 10, 11, 15, 18, 19, 21, and 22) is estimated to be 207 $M_\odot$, which is 56% of the total mass, 372 $M_\odot$. The most striking feature is the filamentary structure of the B213 cloud group consisting of B211, B213, and B216. The cores in the region line up straight at nearly the same interval of ~ 1.1 pc (cores 10, 11, 15, 18, 19, and 21). This filamentary structure is ~ 7 pc in length and ~ 0.5 pc in width. The optical polarization vectors tend to be perpendicular to the filament (Hayer et al. 1987).

L1521.—The total mass of the seven cores (cores, 16, 20, 24, 25, 26, 27, and 28) in this region is estimated to be 157 $M_\odot$, which is 45% of the total mass, 350 $M_\odot$. The column density is small, and the cloud is more extended than the other clouds. The size of core 27 is the largest among all the cores, but the column density is not so large compared to that of the other cores. This may indicate that core 27 has a sheetlike structure. The deviation from the correlation between physical properties discussed later in § 4.2.4 would support this inference.

L1498.—The total mass of the four cores (cores 12, 13, 14, and 17) in this region is estimated to be 58 $M_\odot$, which is 60% of the total mass, 97 $M_\odot$. This is the cloud with the narrowest line widths.

L1506.—There is only one core in this region, and the mass of the core (core 23) is estimated to be 37 $M_\odot$, which is 46% of the total mass, 81 $M_\odot$.

B18.—The total mass of the six cores (cores 29, 30, 31, 33, 35, and 37) in this region is estimated to be 126 $M_\odot$, which is 34% of the total mass, 376 $M_\odot$. This region consists of L1535, TMC-2, and L1524.

HCL2.—The total mass of the three cores (cores 32, 34, and 36) in this region is estimated to be 127 $M_\odot$, which is 15% of the total mass, 843 $M_\odot$. This is the most massive cloud in the observed region. There are double-peaked profiles around the dense parts. It has a ringlike structure, which was explained as a cloud like a "γ-shaped filament" (Cernicharo & Guélin 1987), or an aggregation of the four filamentary components at different velocities (Paper I). However, it is difficult to interpret its kinematics by estimating the ringlike shape because of its complexity in space and velocity.

L1536.—The total mass of the three cores (cores 38, 39, and 40) in this region is estimated to be 42 $M_\odot$, which is 48% of the total mass, 87 $M_\odot$.

4. DISCUSSION

4.1. *Comparison of $C^{18}O$ and ^{13}CO Observations*

Figure 7*a* and 7*b* show the frequency distributions of the peak optical depths of the ^{13}CO and $C^{18}O$ spectra, respectively. For the ^{13}CO spectra (Paper I), 33% of the 12,441 spectra whose intensity is larger than the 3 σ level have optical depths larger than 0.5. For the $C^{18}O$ spectra, such

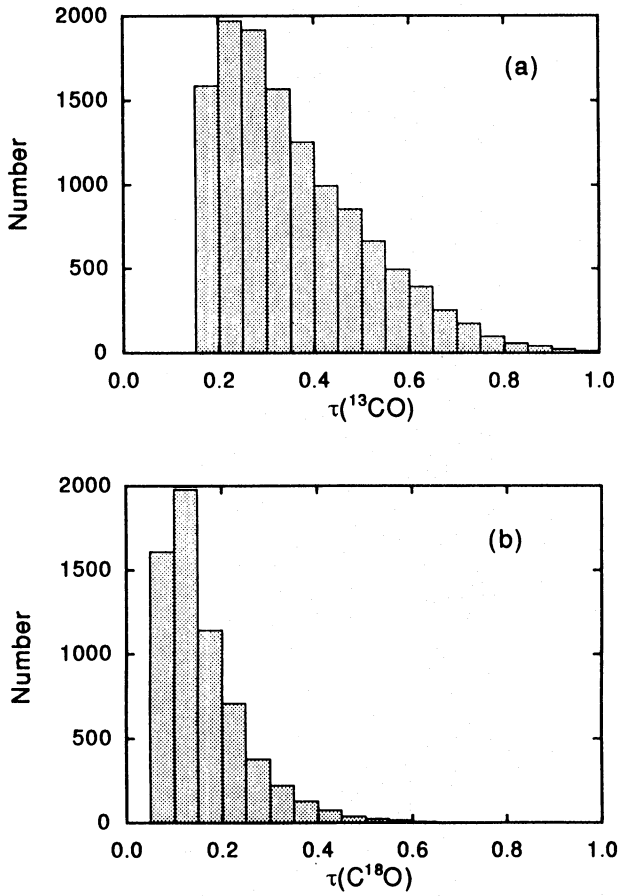

FIG. 7.—The distributions of the optical depth for each observed point. (*a*) Optical depth of ^{13}CO spectra which have integrated intensity of larger than 1.5 K km s^{-1} (5 σ), and (*b*) optical depth of $C^{18}O$ spectra which have integrated intensity of larger than 0.7 K km s^{-1} (5 σ).

spectra having $\tau > 0.5$ represent only 3% of the 6350 spectra. The mean ratio of the optical depth of $C^{18}O$ to that of ^{13}CO is estimated to be 0.35. Thus $C^{18}O$ spectra are considered to be optically thin in almost all the regions observed and to trace high-density regions more accurately than ^{13}CO at a scale down to $\sim$0.1pc.

In order to derive a typical density n of the cloud, we also calculated mean densities within the region in which the integrated intensity is larger than half the maximum integrated intensity in the entire cloud. We divide the mass by the third power of square root of the area to derive the mean density. The mean H_2 density of $C^{18}O$ cloud is then estimated to be $\sim$4000cm^{-3}, which is larger by a factor of $\sim$5 than that of ^{13}CO cloud of $\sim$700 cm^{-3}. Therefore, $C^{18}O$ emission traces a denser region than ^{13}CO emission does by a factor of $\sim$5.

Figure 8 shows the distributions of the equivalent line width (δv), i.e., the integrated intensity divided by the peak temperature of the ^{13}CO and $C^{18}O$ spectra. The mean equivalent line width of the $C^{18}O$ spectra is 0.65 km s^{-1}, which is smaller than that of the ^{13}CO, 1.20 km s^{-1}, by a factor of 2.

The value $n\delta v^2$ for ^{13}CO and $C^{18}O$ obtained by using the typical values for the density and the line width above are $\sim 1 \times 10^{13}$ and $\sim 1.7 \times 10^{13}$ (particles cm^{-1} s^{-2}), respectively. The difference is smaller than a factor of 2. It should be noted that this small difference in these values for ^{13}CO and $C^{18}O$ indicates that the $C^{18}O$ cloud and the ^{13}CO clouds are in pressure balance.

4.2. *Core Properties*

4.2.1. *Mass Spectrum*

We have fitted the mass spectrum of the cores in the mass range from 3 to 80 $M_\odot$ and obtained a spectral index γ of -0.9 ± 0.2 for the present sample. Several authors studied the cloud mass spectrum and determined the spectral index γ for the molecular cloud cores (see, e.g., Blitz 1991 for a review). Some of the derived values of γ are as follows; -1.6 for $M > \sim 20\ M_\odot$ in L1630 (Lada, Bally, & Stark 1991), -1.7 for a range of mass from $\sim$5 to $\sim$160 $M_\odot$ in the Ophiuchus north region (Nozawa et al. 1991), -1.6 ± 0.3 for $M > \sim 50\ M_\odot$ in Orion A (Tatematsu et al. 1993), and -1.6 for $M > \sim 100\ M_\odot$ in the Cygnus region (Dobashi, Bernard, & Fukui 1996). Blitz (1991) suggested that there is a universal power-law mass spectrum for the cloud clumps within a giant molecular cloud (GMC) over the range of more than 3 orders of magnitude and that γ is -1.6 with an uncertainty of $\sim$10%. The present value of γ, -0.8, is significantly different from -1.6, and the mass spectrum is much flatter than the previous ones.

We shall discuss a few possible interpretations on this small index of the present study. One possibility is that the index is different for a different mass range. The masses of the samples in the papers we quote above range up to a larger value than the present sample, and the quoted

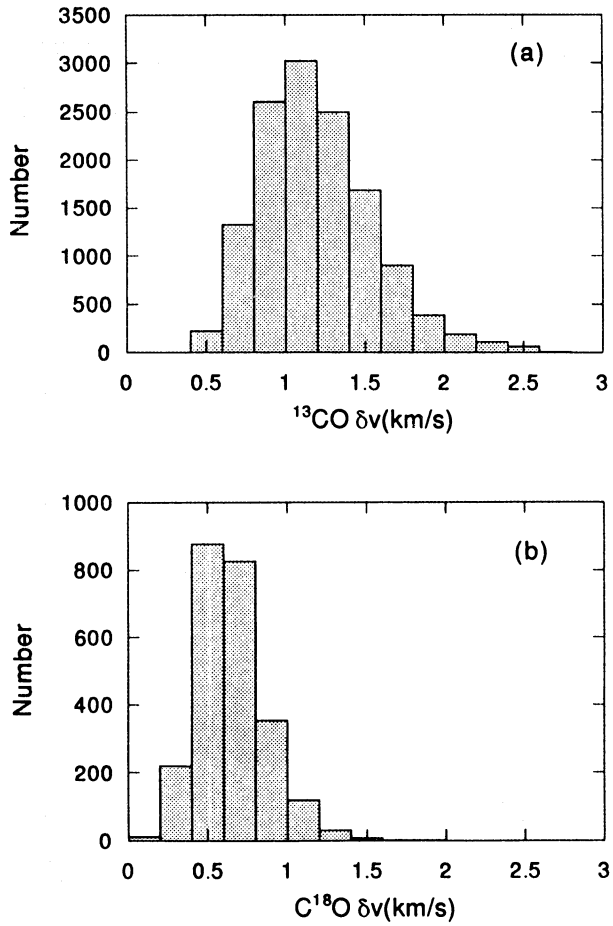

FIG. 8.—Histograms of the equivalent line width (integrated intensity/peak temperature) of (*a*) ^{13}CO and (*b*) $C^{18}O$.

samples were found to be incomplete for the cores for a lower mass. Except for Nozawa et al. (1991), there are no extensive and high-sensitivity surveys of low-mass cores. The spectral index of Nozawa et al. (1991) is -1.7, and we recalculated the spectral index for the low-mass cores whose masses are smaller than 60 $M_\odot$ and estimated it to be -1.1 ± 0.4, which is smaller than the quoted index. The index of the dark cloud cores in Taurus of Myers et al. (1983), whose sample is not necessarily complete, is estimated to be -1.2 ± 0.4, which is also slightly smaller than that of high-mass cores. The mass range is similar to the present sample (from 0.5 to 90 $M_\odot$ except for a cloud of 280 $M_\odot$), although their sampling is incomplete because the cores were selected from visually opaque regions. The index γ for the present sample is -0.4 ± 0.3 for the mass range of $M(M_\odot) = 3 - 25$, and -1.2 ± 0.3 for the range of $M(M_\odot) = 10$–80. Thus, the slope of the spectrum seems to be steeper for a larger mass range. This result indicates that, if a mass spectrum is universal everywhere, an index of the spectrum could change in mass, i.e., large ($\gamma \cong -1.7$) for massive cores and small ($\gamma \cong -0.8$) for low-mass cores. Another interpretation is that the Taurus cloud has a different mass spectrum from the other regions, and the smallness of this index may be unique to the Taurus region. It is important to carry out an unbiased survey of other regions in a wide mass range in order to confirm the universality of the mass spectrum.

4.2.2. *Core Properties in Terms of its Mass*

The mass of a core is nearly proportional to the column density multiplied by the square of the radius. Figure 9 shows a correlation between the radius and the mass of the cores. The straight line indicates a line of constant column density, i.e., $M \propto R^2$. There is a clear positive relation between the size and mass, and the slope becomes steeper

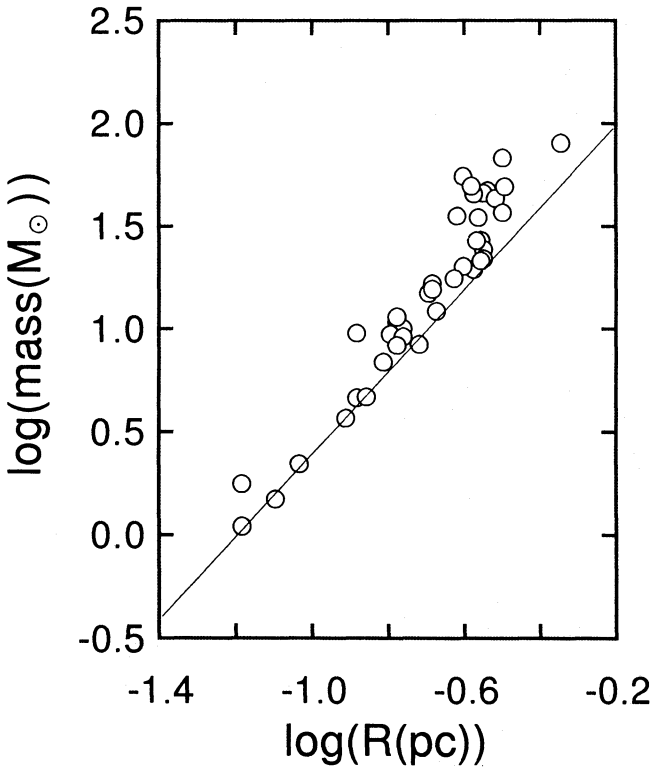

FIG. 9.—Correlation between the mass and the radius of the cores

TABLE 2

PHYSICAL PROPERTIES OF THE LOW-MASS AND HIGH-MASS CORES

PARAMETER	LOW-MASS CORE	HIGH-MASS CORE
Mass ($M_\odot$)	12(8)	50(13)
Δv (km s^{-1})	0.42(0.08)	0.61(0.1)
$N[H_2](10^{21}$ cm$^{-2})$.....	5.6(1.2)	9.9(2.6)
R (pc)	0.18(0.07)	0.30(0.06)
Aspect ratio	1.5(0.4)	2.2(0.3)

NOTE.—Values in parentheses are the standard deviation.

for the cores of a larger size. This plot shows that for the low-mass cores, the mass is proportional to the square of the radius (i.e., the column density is nearly constant) and that for the massive cores, the mass is proportional to the column density. This result indicates that massive cores would tend to have a large size and a larger column density.

We divide the cores into high-mass cores and low-mass cores to characterize the physical properties in terms of mass. Table 2 shows the physical properties of the two categories. The high-mass cores we defined have the mass of >30 $M_\odot$. The high-mass cores have a larger $C^{18}O$ line width, larger size, and, especially, larger column density than those of the low-mass cores. The mean aspect ratio of the high-mass cores is also larger than that of low-mass cores, implying that the high-mass cores tend to have an elongated structure.

4.2.3. *Position Angle*

If cores are not affected by any external force, the frequency distribution of the position angle should be uniform. Previous polarization observations of molecular clouds that have various configurations showed that the magnetic field might influence or be influenced by the configuration of the molecular clouds (Goodman et al. 1990; Myers & Goodman 1991). In some clouds, the polarization vectors are roughly perpendicular to the projected cloud elongation (e.g., B216/217)(Heyer et al. 1987) and Lupus 1(Strom, Strom, & Edwards 1988), and in other clouds they are parallel to the projected cloud elongation (e.g., the B42 cloud in Ophiuchus [Vrba, Strom, & Strom 1976] and L1641 [Vrba, Strom, & Strom 1988]). In Taurus molecular clouds, the polarization vectors are nearly perpendicular to the Galactic plane (Moneti et al. 1984; Heyer et al. 1987; Tamura et al. 1987). Figure 4*e* shows that the mean value of the core position angle is estimated to be $\sim 80°$ and that 70% of the cores have a position angle between 50°–110° ($-20°$). The cores are generally aligned, and therefore the major axis of the core tends to be perpendicular to the polarization vector. This result indicates that the magnetic field affects not only the configuration of the surrounding lower density clouds, but also the formation of the dense molecular cloud cores which have $n(H_2) \sim 10^4$ cm^{-3} on a scale of 0.1 pc.

4.2.4. *Line Width*

The line width tells us about internal kinematical properties of cores like thermal motion and turbulence. Figures 10–11 show correlations among the line width and other properties of the cores. Figure 10*a* shows a correlation between the mass and observed line width of the cores. It is clear that the cores with mass of >20 $M_\odot$ except for core 27 show an increase of the line width with the mass. For the cores with mass of >20 $M_\odot$ except for core 27, a linear fit to

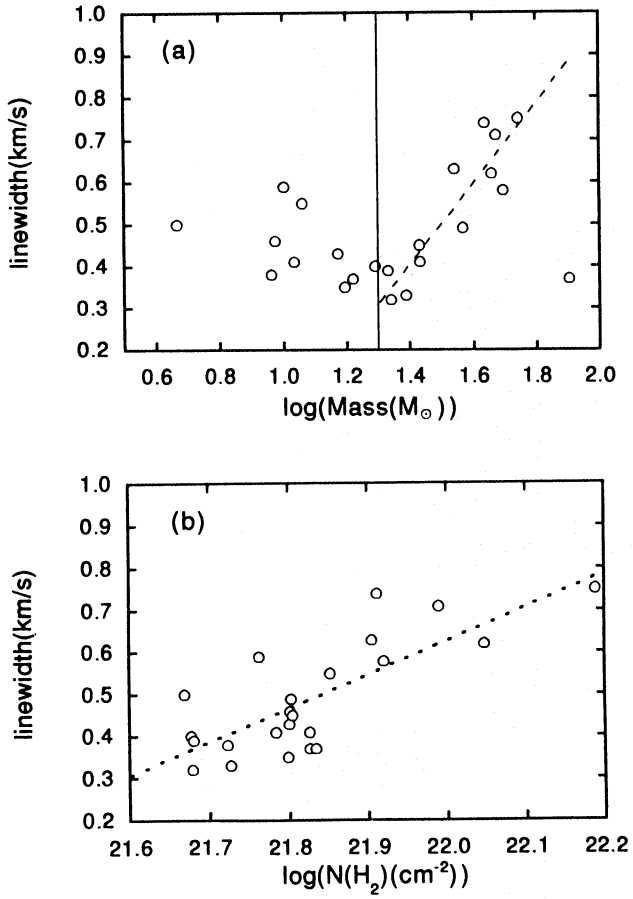

FIG. 10.—(*a*) Correlation between the mass and the line width of the cores. Dashed line is the best-fit line for the cores with mass of $>20\ M_\odot$ (*vertical straight line*). (*b*) Correlation between the H_2 column density and the line width of the cores. Dashed line is the best fit for the cores.

the data gives the equation

$$\Delta v_{\rm obs} = (0.9 \pm 0.1) \log (M) - (0.9 \pm 0.2), \quad {\rm CC} = 0.85 ,$$

where $M(M_\odot)$ is the mass of the core, $\Delta v_{\rm obs}$ is the $C^{18}O$ line width, and CC is the Spearman rank correlation coefficient. The uncertainties are a standard deviation. The deviation of core 27 from the correlation supports the possibility that the core has a sheetlike structure as shown in §3.2. For the cores having mass less than 20 $M_\odot$, there seems to be a negative correlation or no correlation between the mass and line width, although we need more samples to confirm this result. Figure 10*b* shows a correlation between the column density and the line width. A linear fit to the data gives the equation

$$\Delta v_{\rm obs} = (0.8 \pm 0.1) \log (N) - (17 \pm 3), \quad {\rm CC} = 0.63 ,$$

where N is the column density of the H_2. Therefore, the cores show a statistically significant increase of the column density with the line width, although the correlation is not so strong.

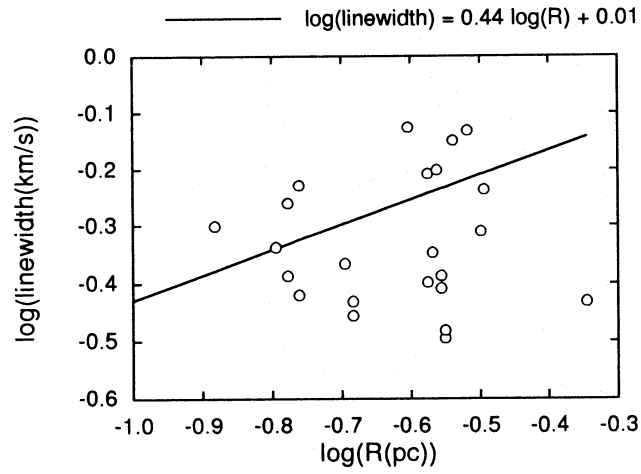

FIG. 11.—Correlation between the radius and the line width of the cores. The straight line is the correlation for the starless cores of Fuller & Myers (1992).

Several authors have suggested that there is a relation between a line width of the spectrum and a size of a core in the form of $\Delta v_{\rm obs} \propto R^p$; $\Delta v_{\rm obs}$ is a characteristic velocity width of an observed spectrum, and R means a characteristic size of a core or a cloud (e.g., Larson 1981; Leung, Kutner, & Mead 1982; Myers 1983; Myers, Ladd, & Fuller 1991). The origin of this relation, however, is not well known. Larson (1981) pointed out that the size and line width of a molecular cloud have a relation, $\Delta v_{\rm obs} \propto R^{0.38}$, over a wide range in size from 0.1 to 100 pc. Fuller & Myers (1992) determined this relation from observations of the CS, $C^{18}O$, and NH_3 lines in 14 dense cores and found a relation $\Delta v_{\rm obs} \propto R^{0.4 \pm 0.1}$ in a scale size from 0.02 to 0.36 pc. To investigate the relationship between the line width and size in the Taurus, we plotted the core radius versus the line width (Fig. 11). A linear fit to the data gives the equation

$$\log (\Delta v_{\rm obs} = (0.0 \pm 0.2) \log (R) - (0.3 \pm 0.1) ,$$

$$\rm CC = 4 \times 10^{-4} .$$

This suggests no correlation between the line width and size.

There are two possible interpretations of this behavior. One is that there is in fact no line width–size relation. Some authors have questioned the relation, and it has been suggested that the correlation may be due to the selection effects (e.g., Blitz 1988; Kegel 1989). Another interpretation is that there is actually a line width–size relation. The present sample has only a small dynamic range in cloud size, ranging from 0.13 to 0.4 pc. The straight line in Figure 11 indicates the relation of Fuller & Myers (1992). Although there seems to be no correlation between the line width and size from the present data, the data are distributed around the line obtained by Fuller & Myers (1992). This result may indicate that we see only the cores in a small dynamic range of cloud sizes, although there is a relation in a large dynamic range in size ranging over 3 orders of magnitude.

For a spherical uniform density cloud of mass $M(M_\odot)$, radius R(pc), and linewidth $\Delta v_{\rm obs}$, virial theorem implies

$$M = 210\ R\ \Delta v_{\rm obs}^2 .$$

The ratio $M/(210R\ \Delta v_{\rm obs}^2)$ has been calculated for the cores and plotted versus mass in Figure 12. If a core has a spherical shape and is in virial equilibrium, the ratio must be constant in mass and nearly equal to one. The ratio of core 27 is apparently larger than that of the other cores, which is consistent with the shape of the core. A linear fit to the data except for core 27 gives the equation

$$\log [M/(210R\ \Delta v_{\rm obs}^2)] = (0.1 \pm 0.1) \log M + (0.1 \pm 0.2) ,$$

$$\rm CC = 0.18 .$$

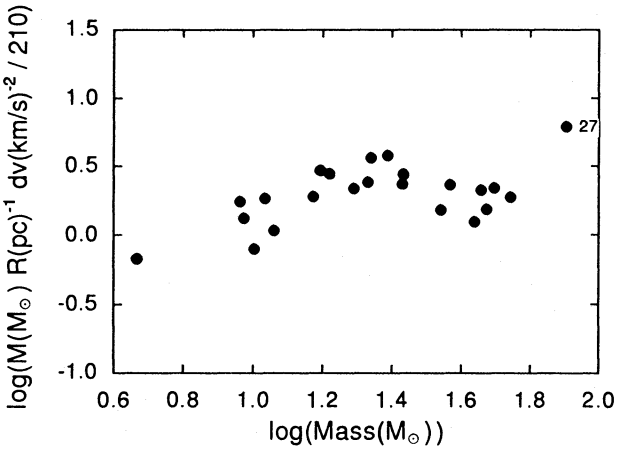

FIG. 12.—The virial ratio $M(M_\odot)R(\mathrm{pc})^{-1}dv(\mathrm{km\ s^{-1}})^{-2}/210$ vs. mass of the cores.

The standard deviation of $\log [M/(210R\ \Delta v^2_{\mathrm{obs}})]$ is 0.2. Therefore, we can conclude that most of the cores observed are roughly gravitationally bound and at least approximately in virial equilibrium.

5. CONCLUSIONS

The observations were carried out toward the Taurus molecular cloud in the $C^{18}O$ ($J = 1$–0) line at a linear resolution of 0.1 pc and revealed the whole structure of the Taurus molecular cloud of density $n(H_2) \sim 10^3$–10^4 cm^{-3} at a scale of 0.1 pc for the first time.

The major conclusions of this paper are as follows.

1. The total mass of the $C^{18}O$ cloud is estimated to be 2900 $M_\odot$, which is ~43% of the mass derived from the ^{13}CO observations.

2. The mean and maximum values of the optical depth of the $C^{18}O$ ($J = 1$–0) line are estimated to be 0.35 and 0.9, respectively. The optical depth of the $C^{18}O$ emission is calculated to be smaller than that of ^{13}CO, and the $C^{18}O$ emission is considered to be optically thin in almost the entire region at a size scale down to ~0.1 pc.

3. We identified 40 dense cores, a sample of the dense molecular gas of $n(H_2) \sim 10^4$ cm^{-3}, whose mass ranges from 1 to 80 $M_\odot$. The typical $C^{18}O$ core has radius 0.23 pc, line width 0.49 km s^{-1}, column density 6.9×10^{21} cm^{-2}, and mass 23 $M_\odot$.

4. The mass spectrum of the cores is fitted by a power law with index -0.9 ± 0.2, which is a significantly smaller value than those of the previous surveys.

5. The major axis of the cores tends to be aligned parallel to the Galactic plane, although the magnetic fields are roughly perpendicular to the Galactic plane. This result indicates that an overall magnetic field affects the formation of dense cores of $n(H_2) \sim 10^4$ cm^{-3}.

6. An analysis of correlations among the physical quantities of the cores indicates that the line width has a positive correlation with the mass and column density of the cores, but not with the size in a range from 0.13 pc to 0.45 pc in radius. Most of the cores observed are roughly gravitationally bound and at least approximately in virial equilibrium.

We are grateful to K. Dobashi for his helpful comments. T. O. is supported financially by the Japan Society for the Promotion of Science. This research was supported financially in part by the Scientific Research Fund of the Ministry of Education, Science, and Culture, Japan, under grant no. 05402003, 07404008 (Y. F.) and 06452020 (A. M.), and by the Sumitomo Foundation No. 94-103-1013 (A. M.).

REFERENCES

Barnard, E. E. 1927, A Photographic Atlas of Selected Regions of the Milky Way, ed. E. B. Frost, & M. R. Calvert (Washington, DC: Carnegie Inst. of Washington)
Beichman, C. A., Myers, P. C., Emerson, J. P., Harris, S., Mathieu, R., Benson, P. J., & Jennings, R. E. 1986, ApJ, 307, 337
Benson, P. J., & Myers, P. C. 1989, ApJS, 71, 89
Blitz, L. 1988, in Millimeter and Submillimeter Astronomy, ed. R. D. Wolstencroft & W. B. Burton (Dordrecht: Kluwer), 269
———. 1991, in The Physics of Star Formation and Early Stellar Evolution, ed. C. J. Lada and N. D. Kylafis (Dordrecht: Kluwer), 3
Cernicharo, J., & Guélin, M. 1987, A&A, 176, 299
Cohen, M., & Kuhi, L. V. 1989, ApJS, 41, 743
Dobashi, K., Bernard, J. P., & Fukui, Y. 1996, ApJ, in press
Dutrey, A., Langer, W. D., Bally, J., Duvert, A., & Wilson, R. W. 1991, A&A, 247, L9
Duvert, G., Cernicharo, J., & Baudry, A. 1986, A&A, 164, 349
Elias, J. H. 1978, ApJ, 224, 857
Frerking, M. A., Langer, W. D., & Wilson, R. W. 1982, ApJ, 262, 590
Fukui, Y., Mizuno, A., Nagahama, T., Imaoka, K., & Ogawa, H. 1991, Mem. Soc. Astron. Italiana, 62, 801
Fukui, Y., et al. 1994, in The Cold Universe, ed. Th. Montmerle et al. (Gif-sur-Yvette Cedex: Editions Frontiéres), 157
Fuller, G. A., & Myers, P. C. 1992, ApJ, 384, 523
Goodman, A. A., Bastien, P., Myers, P. C., & Ménard, F. 1990, ApJ, 359, 363
Herbig, G. H., & Bell, K. R. 1988, Lick Obs. Bull. Ser., No. 1111
Heyer, M. H., Vrba, F. J., Snell, R. L., Schloerb, F. P., Strom, S. E., Goldsmith, P. F., & Strom, K. M. 1987, ApJ, 321, 855
IRAS Point Source Catalog, Version 2, 1988, Joint IRAS Science Working Group (Washington, DC: GPO)
Jones, B. F., & Herbig, G. H. 1979, AJ, 84, 1872
Kegel, W. H. 1989, A&A, 225, 517
Lada, E. A., Bally, J., & Stark, A. A. 1991, ApJ, 368, 432
Larson, R. B. 1981, MNRAS, 194, 809
Leung, C. M., Kutner, M. L., & Mead, K. N. 1982, ApJ, 262, 583
Lynds, B. T. 1962, ApJS, 7, 1
Mizuno, A., Onishi, T., Hayashi, M., Ohashi, N., Sunada, K., Hasegawa, T., & Fukui, Y. 1994, Nature, 368, 719
Mizuno, A., Onishi, T., Yonekura, Y., Nagahama, T., Ogawa, H., & Fukui, Y. 1995, ApJ, 445, L161 (Paper I)
Moneti, A., Pipher, J. L., Helfer, H. L., McMillan, R. S., & Perry, M. L. 1984, ApJ, 282, 508
Myers, P. C. 1983, ApJ, 270, 105
Myers, P. C., & Goodman, A. A. 1991, ApJ, 373, 509
Myers, P. C., Ladd, E. F., & Fuller, G. A. 1991, ApJ, 372, L95
Myers, P. C., Linke, R. A., & Benson, P. J. 1983, ApJ, 264, 517
Nercessian, E., Castets, A., Cernicharo, J., & Benayoun, J. J. 1988, A&A, 189, 207
Nozawa, S., Mizuno, A., Teshima, Y., Ogawa, H., & Fukui, Y. 1991, ApJS, 77, 647
Ogawa, H., Mizuno, A., Hoko, H., Ishikawa, H., & Fukui, Y. 1990, Int. J. Infrared Millimeter Waves, 11, 717
Onishi, T., Mizuno, A., Kawamura, A., Ogawa, H., & Fukui, Y. 1996, ApJ, submitted
Schloerb, F. P., & Snell, R. L. 1984, ApJ, 283, 129
Strom, S. E., Strom, K. M., & Edwards, S. 1988, in Galactic and Extragalactic Star Formation, ed. R. E. Pudritz & M. Fich (Dodrecht: Kluwer), 53
Tamura, M., Nagata, T., Sato, S., & Tanaka, T. 1987, MNRAS, 224, 413
Tatematsu, K., et al. 1993, ApJ, 404, 643
Ungerechts, H., & Thaddeus, P. 1987, ApJS, 63, 645
Vrba, F. J., Strom, S. E., & Strom, K. M. 1976, AJ, 81, 958
———. 1988, AJ, 96, 680
Wilking, B. A., & Lada, C. J. 1983, ApJ, 274, 698
Zhou, S., Wu, Y., Evans, N. J., Fuller, G. A., & Myers, P. C. 1989, ApJ, 346, 168